

Long-term X-ray monitoring of LS I +61°303: analysis of spectral variability and flares

Jian Li¹, Diego F. Torres^{2,3}, Shu Zhang¹, Yupeng Chen¹, Daniela Hadasch³, Paul S. Ray⁴,
Peter Kretschmar⁵, Nanda Rea³, & Jianmin Wang^{1,6}

ABSTRACT

We report on the full analysis of a *Rossi X-ray Timing Explorer* (*RXTE*) Proportional Counter Array (PCA) monitoring of the γ -ray binary system LS I +61°303. The data set covers 42 contiguous cycles of the system orbital motion. Analyzing this X-ray monitoring dataset, the largest to date for this source, we report on the variability of the orbital profile and the spectral distribution, and provide strong evidence for an anti-correlation between flux and spectral index (the higher the flux, the harder the spectral index). Furthermore, we present the analysis of two newly discovered ks-timescale flares, which present significant variability also on shorter timescales, and tend to occur at orbital phases between 0.6-0.9. However, a detailed timing analysis of the flares does not show any coherent or quasi-coherent (QPO) structure in their power spectra. We also investigated the possible appearance of the radio super-orbital modulation at X-rays energies, but we could not unambiguously detect such modulation in the system flux history, nor in the evolution of its orbital modulation fraction.

Subject headings: X-rays: binaries, X-rays: individual (LS I +61°303)

1. Introduction

Among the class of X-ray binaries, LS I +61°303 is peculiar because it was detected in all energy ranges from radio to TeV. The other binary systems with somewhat similar

¹Laboratory for Particle Astrophysics, Institute of High Energy Physics, Beijing 100049, China. Email: jianli@ihep.ac.cn

²Institució Catalana de Recerca i Estudis Avançats (ICREA).

³Institut de Ciències de l'Espai (IEEC-CSIC), Campus UAB, Torre C5, 2a planta, 08193 Barcelona, Spain

⁴Space Science Division, Naval Research Laboratory, Washington, DC 20375-5352

⁵ESA-European Space Astronomy Centre, 28691 Villanueva de la Cañada, Madrid, Spain

⁶Theoretical Physics Center for Science Facilities (TPCSF), CAS, China

characteristics are PSR B1259-63 (Aharonian et al. 2005b), a system hosting a pulsar, and Cyg X-1 (Albert et al. 2007), a system most likely hosting a black hole, and LS 5039 (Aharonian et al. 2005a, Aharonian et al. 2006). The nature of the compact object in both LS 5039 and LS I +61°303 remains unknown. We do know that LS I +61°303 consists of a rapidly rotating B0 Ve star with an equatorial outflowing disk orbited by a low mass ($M \sim 1-4 M_{\odot}$) compact object with a period of ~ 26.5 days in an eccentric orbit (see Casares et al. 2005; Grundstrom et al. 2007; Aragona et al. 2009). This periodicity is visible in the optical band (Hutchings & Crampton 1981, Mendelson & Mazeh 1989), in the infrared (Paredes et al. 1994), in soft X-rays (Paredes et al. 1997), in the H_{α} emission line (Zamanov et al. 1999), and in the high-energy band (20 MeV–100 GeV; Abdo et al. 2009). The radio outbursts not only show this 26.5 day periodicity but also a shift of the phase of the radio maximum between $0.45 \leq \Phi \leq 0.9$, with a 1667 ± 8 day second modulation (Gregory 2002). In the X-ray band, a number of observational campaigns have been carried out, showing that the emission is variable and has a non-thermal spectrum. Two simultaneous X-ray and radio observations showed that the X-ray emission peaks almost half an orbit before the radio and, in both bands, the orbital phases of the flux maxima seemingly drift from orbit-to-orbit (Taylor et al. 1996; Harrison 2000). However, soft X-ray pointed observations of LS I +61°303 have in general been too limited to cover full orbits of the system or to study long-term evolution of the X-ray orbital profile. This limitation was recently removed by the work of Torres et al. (2010, referred here as Paper I) who showed that the periodic behavior is visible only over long integration times and that profile variability is seen from orbit-to-orbit all the way up to multi-year timescales, with the phase of the profile maximum also changing.

To explain the behavior and constituency of LS I +61°303 there are two major models: 1) Accretion onto a compact object, a black hole or a neutron star (Taylor & Gregory 1984), and 2) Interaction of a young rotation powered pulsar with the wind from the companion Be star (Maraschi & Treves 1981). Both Sidoli et al. (2006) and Rea et al. (2010) searched for evidence of pulsations (which in principle could support either model) but found none. To prove the accretion model, one should make direct measurements of accretion signatures or of jet like structures. In 2004, Massi et al. (2004) reported on the existence of a large-scale persistent radio jet. But Albert et al. (2008) did not find any such jet at any of the scales explored using radio interferometric observations from the MERLIN, EVN, and VLBA arrays in 2006. In radio images of LS I +61°303 obtained during a complete orbital cycle, Dhawan et al. (2006) saw an extended feature, which they ascribed to a cometary tail that changes orientation along the orbit. The same structure was confirmed several months later by Albert et al. (2008). But neither of these imaging studies found a clear evidence for a jet. Another proof for the accretion/jet models would be the discovery of a cutoff

in the 10–100 keV energy spectrum. But studies made by Chernyakova et al. (2006) with *XMM-Newton* and *INTEGRAL* data could not bring this proof. Recent investigations on a much larger *INTEGRAL* dataset reached the same conclusion (Zhang et al. 2010). The data could be fitted well by a simple power law without features, matching to the higher energy spectrum in the 100 keV–10 MeV band found with OSSE (Tavani et al. 1996) and COMPTEL (van Dijk et al. 1996). If the system is an accreting neutron star or black hole, one expects to find a cut-off power-law spectrum in the hard X-ray band with a cut-off energy normally at 10–60 keV for neutron stars (e.g. Filippova et al. 2005) and at ~ 100 keV for black holes (McClintock & Remillard 2003). Even when one can think of situations where the accretion disc is masked by a jet component, producing a featureless power law, if the accretion flow and the jet would give comparable contributions in the hard X-ray band, one would still expect at least a feature in the *INTEGRAL* energy range, due to the disappearance of contribution of the disc at high energies (see e.g., Chernyakova et al. 2006, Zhang et al. 2010). Sidoli et al. (2006) could not find proofs for accretion either, although they found (in *XMM-Newton* and BeppoSAX observations) evidence for a rapid change in flux in timescales of hours. This behavior has also been observed in *Chandra* data (Paredes et al. 2007, Rea et al. 2010). Esposito et al. (2007) carried out a *Swift*/XRT monitoring, observing flux fluctuations up to a factor of 3 at intra-hour scales, but once again, finding no emission or absorption lines in the spectrum. An *RXTE* long-term monitoring, from August 28 2007 to February 2 2008 (a dataset which is included in our analysis) was presented by Smith et al. (2009). They hinted at a correlation between the flux and photon index, with the spectrum becoming harder at higher fluxes. Furthermore they hinted at the orbital modulation, peaking at phases 0.6–0.7 as claimed by Paredes et al. (1997) and Esposito et al. (2007), which was seemingly not smooth, but presented short-timescale flares and very strong orbit-to-orbit variability. The short time intervals covered in these publications did not permit strict conclusions, some of which were later to be claimed in Paper I and are studied in more detail here.

Finally, we remark that LS I +61°303 has also been extensively studied in the very high energy range (VHE). The MAGIC collaboration first detected LS I +61°303 as a variable TeV source, which was independently confirmed by the VERITAS collaboration (Albert J. et al. 2006; Acciari et al. 2008). Both experiments found TeV emission only near the apastron passage of the compact object in its orbit around the Be star. The MAGIC collaboration conducted a multiwavelength campaign including the MAGIC telescope, *XMM-Newton* and *Swift* during 60% of an orbit in 2007 September (Anderhub et al. 2009). They discovered an X-ray/VHE gamma-ray correlation during an outburst around orbital phase 0.62, while the uncertainties prevent to be sure about the existence of the correlation outside the outburst. Again, this conclusion was also derived by the VERITAS collaboration, when reporting the

lack of X-ray/VHE correlation based on contemporaneous data with a VHE sampling that is not dense enough (Acciari et al. 2009). LS I +61°303 even seems to have disappeared in the VHE band during quite some time, following recent results presented by VERITAS (Aliu et al. 2010, see below).

Long-term and especially continuous monitoring of gamma-ray binaries has been a goal for many years, so that we can start to see differences between them that could help us distinguish their nature, the possible distinct influence of the companion star, and the possible variability expected at other frequencies where only snapshots are possible. Long-term monitoring provides information on possible trends in the overall behavior of the source, and gives perspective as of the steadiness or variability of the former conclusion. Such monitoring can also catch unusual events or source states, or duty cycles, that could provide the key to the nature of the source. There are a few potential observations that one may think would conclusively demonstrate the true nature, such as the discovery of pulsations at any frequency or the detection of clear accretion signals like accretion lines, both of which are for the moment still elusive (see, e.g., Rea et al. 2010). Multifrequency observations can provide knowledge of the dominance of single or multiple particle populations, and of the nature of these particles. Thus, several questions can be tackled with this campaign. Some examples are whether the hinted anti-correlation between spectral index and flux is real, whether it changes with time if so, whether the spectra deviates from a pure absorbed power law along the different observation timescales, whether the anti-correlation between flux and spectral index is also present in flares, whether the modulation fraction varies, whether there were additional flares from the source, whether they come at particular phases of the orbit and which is their inner structure, whether they had timing signatures, and others. We tackle these questions here.

This paper is thus a detailed follow up of Paper I, presenting the full analysis of the largest dataset on LS I +61°303 obtained in soft X-rays to date, enlarging that used in Paper I by several orbits, and concentrating on the spectral behavior of the source. Analyzing this X-ray monitoring dataset, we report on the variability of the orbital and spectral profiles, and on an anti-correlation between flux and spectral index (the higher the flux, the harder the spectral index). Furthermore, we present timing analysis of two discovered flares, for which do not show any peculiar feature in their power spectra. These flares, given the PCA field of view, may or may not be associated with LS I +61°303. However, we analyze all flares together (a total of 5 are known coming from the general direction of the system) and find circumstantial evidence for an association.

2. Observations and data analysis

Our dataset covers the period between 2006 October and 2010 September, containing and enlarging the data used for Paper I and it includes 378 *RXTE*/PCA pointed observations identified by proposal numbers 92418, 93017, 93100, 93101, 93102, 94102 and 95102. As in Paper I, here we focus on the data starting on 2007 September because of the smaller time gaps between observations, providing a total exposure time of 549 ks on the source.

In the analysis of PCA data two separate data modes were used: the “Standard 2” mode was used for lightcurve and spectral analysis with 16s accumulation time and 129 energy channels; for analysis of flares, which required greater time resolution, the “Good Xenon” mode was utilized with 1 μ s resolution, and 256 energy channels. Data reduction in both modes was performed using HEASoft 6.6. For the Standard 2 analysis we filtered the data using the standard *RXTE*/PCA criteria. As explained by Smith et al. (2009), since combining large spectral data sets with differing PCA configurations (with associated differing calibrations) can produce large systematic errors, it is preferable to use a single common PCU for all available data sets. PCU2 (in the 0–4 numbering scheme) is used for most of the analysis as it was the only PCU that was 100% on during the observations. We select time intervals where the source elevation is $> 10^\circ$ and the pointing offset is $< 0.02^\circ$. PCA background lightcurves and spectra were generated using FTOOLS task `pcabackest`. `pcarsp` is used to generate PCA response matrices for spectra. The background file used in analysis of PCA data is the most recent available from the HEASARC website for faint sources, and detector breakdown events have been removed.¹

As stated, we have analyzed the flares using Good Xenon data which are also barycentered using the FTOOLS routine `faxbary` assuming in this process that they come from LS I +61°303. We caution that the PCA field of view is about 1 degree (FWHM) thus providing no direct evidence for the relation of this flaring phenomenology with LS I +61°303. Since none of these short flares were observed by any instrument with a better spatial resolution, we cannot exclude that they were generated in a nearby (in sky projection) source. During the observations of the two new flares – at about MJD 54670.844444 and MJD 54699.653333 – PCU 3 and 4 were on as well. To include more photons, lightcurves and spectra from top layers of PCU 2, 3, and 4 were extracted from 3–10 keV. Above 10 keV, there was a severe lack of photons leading to large error bars in the energy spectrum that

¹The background file is `pca_bkgd_cmfaint17_eMv20051128.mdl` and see the website: http://heasarc.gsfc.nasa.gov/docs/xte/recipes/pca_breakdown.html for more information on the breakdowns. The data have been barycentered using the FTOOLS routine `faxbary` using the JPL DE405 solar system ephemeris.

were not proper for fitting. Background subtraction for Good Xenon lightcurves was carried out using the FTOOLS task `lcmath`: it subtracts a background lightcurve produced from Standard 2 data with the same combination of PCUs and the same energy range which was carried out by using FTOOLS task `lcmath`. Timing analysis of 0.01 seconds binned lightcurves was carried out using `powspec`, producing power spectra in the range from 0.1 to 50 Hz.

3. Results

3.1. Spectral analysis

In the top panel of Figure 1, we show the count rate in 64 second time bins in the 3–10 keV band over the observation period. For each observational ID, a simple power law shape, with absorbing hydrogen column density fixed at $0.75 \times 10^{22} \text{ cm}^{-2}$ (Kalberla et al. 2005, Smith et al. 2009), was used to fit the Standard 2 data. We adopt this most recent determination of N_H and the spectral fit used is

$$N(E) = K e^{-N_H \sigma(E)} \left(\frac{E}{\text{keV}} \right)^{-\alpha}, \quad (1)$$

where K is a normalization at 1 keV, σ is the photoelectric cross section and α is the photon index, referred to as slope. Higher values of alpha are referred to as being *soft* and lower values as being *hard*. The flux values were obtained by integrating the best fit spectra and 1σ error levels were generated. In Figure 1, we show this derived flux and the photon index in the second and third panels. The reduced χ^2 values for the fit are also shown in Figure 1: there are 368 data points averaging around 0.60 ± 0.01 . All errors in this paper are reported in a significance of 1σ .

As previously seen in Paper I, the lightcurve shows two new flares in addition of the three events previously reported by Smith et al.(2009). The average flux value in energy units, plotted in the second panel of Figure 1, is $(1.024 \pm 0.004) \times 10^{-11} \text{ erg cm}^{-2} \text{ s}^{-1}$. Whereas fitting a constant to the lightcurve shows obvious variability of the flux (the reduced χ^2 is $1.3 \times 10^4 / 367$), the variability in the spectral index appears only moderate. This can be seen in the third panel of Figure 1: the reduced χ^2 of a horizontal line is $426 / 367$ and corresponds to the spectral index being a non-zero constant value during the observational period with a significance of $\sim 2.4\sigma$. The spectral index averaged over the all *RXTE*/PCA observations is 1.876 ± 0.012 .

In order to produce orbital profiles, we folded the data by the measured radio period of 26.4960 ± 0.0028 days (Gregory 2002) and an orbital zero phase at MJD 43366.275 (Gregory

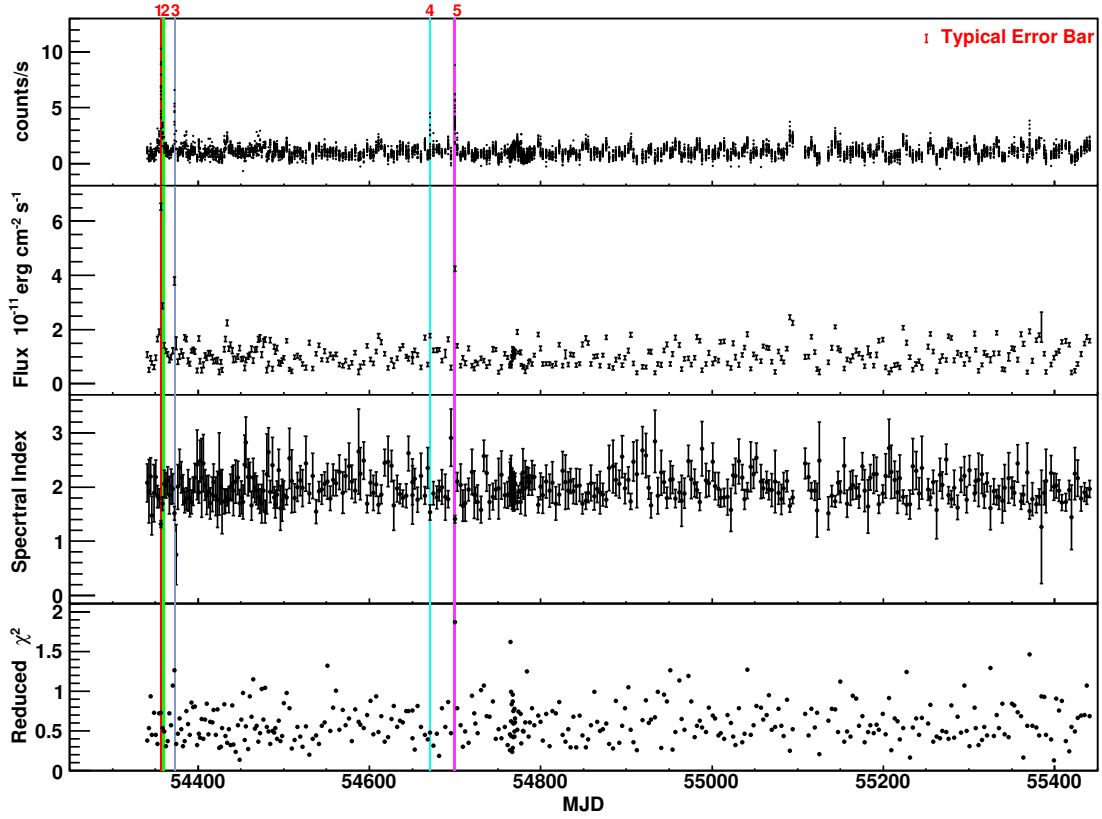


Fig. 1.— 3–10 keV PCA count rate (first panel), observed flux in the 3–10 keV energy band (second panel), spectral index (third panel), and reduced χ^2 (lower panel) from fitting each observational ID with a powerlaw function. Details are provided in the text. The vertical lines report on the flares periods; the last two are separately analyzed in the text.

& Taylor 1978) and then divided the data into 10 orbital phase bins. Figure 2 shows these orbital profiles for the data both with (top row) and without (bottom row) the 5 flares. The left panels show the flux vs. phase, the middle show spectral index vs. phase, and the right panels show spectral index vs flux for the 10 phase bins. A clear orbital modulation can be seen in the flux data (see left panels of Figure 2), with a peak rising up around phase 0.45. This phase is shortly after the periastron passage, which is between phase 0.23–0.30 (Casares et al. 2005; Aragona et al. 2009; Grundstrom et al. 2007). Note in the top middle panel of Figure 2 that there is a very hard value of the spectral index in the phase bin 0.7–0.8. This dip is due to two flares with a very hard spectral slope that reduce the average value of the slope in this bin. In the right panel of Figure 2, we show a clear anti-correlation between flux and spectral index, i.e., the higher the flux, the harder the spectral index. Smith et al. (2009) also hinted at an anti-correlation between the flux and the spectral index but

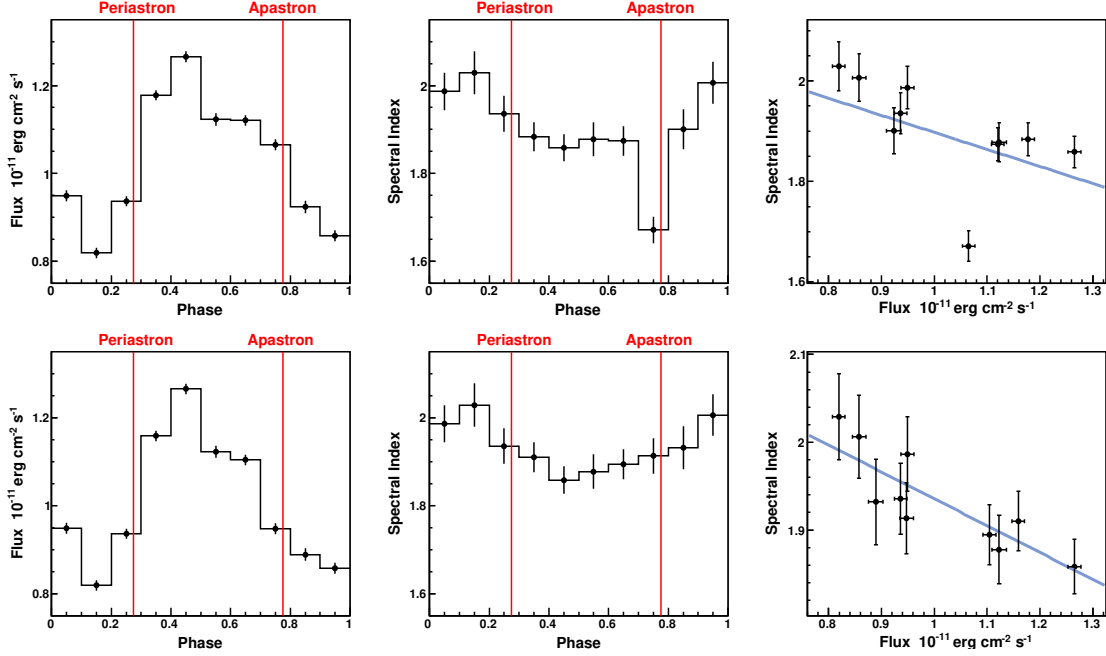


Fig. 2.— Top: The folded orbital profile for the 3–10 keV flux (left) and spectral index (middle) derived for all *RXTE* data (including the flares periods). The rightmost panel represents the relation between the values of the spectral index and the flux determined for each of the 10 phase bins in which the orbit was divided. The line is a linear fit to the data as described in the text. Bottom: Same as the top panels but excluding the 5 flares from the data.

using only *RXTE* data covering the 2007–2008 campaign (MJD 54340–54500). This entire campaign is included in our study and we explore this anti-correlation with this much larger dataset. In the rightmost panel of Figure 2, we show a linear fit to the data. In the top right panel (flares included), the linear fit has a reduced χ^2 of 57.4/8 and a slope of -0.34 ± 0.1 while in the bottom right panel (flares excluded), the linear fit has a reduced χ^2 of 4.2/8 and a slope of -0.31 ± 0.1 .

Figure 3 explores this flux-spectral index anticorrelation for the entire data set. The left panel shows all data, the middle panel excludes the 5 flares, and the right panel shows data for the 5 flares only. From left to right, the linear fits to the data have a slope of -0.14 ± 0.01 , with a reduced χ^2 of 221.3/366; -0.26 ± 0.03 , with a reduced χ^2 of 192.9/361; and -0.06 ± 0.03 , with a reduced χ^2 of 2.4/3.

Note that the two observation IDs with very low value of spectral index and larger error bars, 93100-01-18-00 and 95102-01-54-00, are located at MJD 54374.15621064 and MJD

55384.41457248. In these observations, the good time intervals are only 160 s and 32 s respectively, quite smaller than the typical 1000 – 2000 s of good time intervals obtained for the other data points. As a result, few photons are accumulated in these short intervals, so the data points in the energy spectrum have larger error bars and we cannot derive a good and reliable fit, even when the χ^2 -value is small due to the errors. As a result of the unreliable fit in these two observations, we exclude these data from our analysis below. To be sure that the found anti-correlation is not spurious, we carefully examined two sources of bias: 1) systematic uncertainties in the estimated background spectrum, and 2) extraction of the flux from the fitted spectrum. Especially around 10 keV and above, the background accounts for a large fraction of the observed counts. Thus, a small error in the background subtraction can have a large impact on the net counts of the source, which especially for weak sources may lead to a significant change in the spectral index. By using the `corfile` and `cornorm` commands in `Xspec`, we estimated the largest uncertainty that may result from possible improper background subtraction and found that the fitted fluxes and spectral indices, as well as their anticorrelation, are not significantly affected. To check for effects of this second possible bias, we extracted the lightcurves in count rate for each observation and found that the count rate versus the spectral index can be fitted by the same linear fits as noted. The Pearson product-moment correlation coefficient² of all data including flare points is $-0.50^{+0.04}_{-0.04}$, for data without flares it is $-0.50^{+0.04}_{-0.04}$, and for flare points only it is $-0.67^{+0.57}_{-0.24}$ (errors correspond to 1σ level). Taking into account the non-linearity of errors, we find that the correlation coefficient is different from zero by 10.45σ in the first case, by 10.50σ in the second (no flares) case, and by 1.1σ in the third (only flares) case. Therefore, we again can conclude that there is a significant anti-correlation between the spectral index and the flux using all data or just the data without the flares. However, looking at the flares only, no anti-correlation can be claimed.

Comparing these three plots, one can conclude that the anti-correlation is an orbit-associated effect, with less presence in the flares. The data for the flares show that an increase in flux by a factor of 3 can still be fitted by the same spectral index as the non-flare data. This is not the case for the orbital-associated X-ray emission. This difference could indicate that either the process generating the flares is not the same from the usual X-ray emission of the source, or that the origin of the flares is not LS I +61°303. We caution however that an alternative explanation to this, which is further explored below, is that the resulting behavior is a consequence of a single power law fit across the flare, when in reality,

² See ‘Numerical recipes in C’ available online at <http://www.fizyka.umk.pl/nrbook/bookcpdf.html> and especially, Chapter 14.5 Linear Correlation for the coding tool, and Smith et al. 2009 or Albert et al. 2007b for applications.

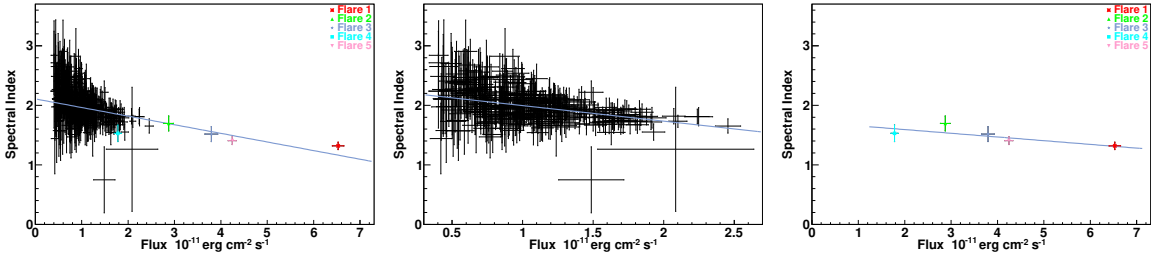


Fig. 3.— Spectral index vs. flux for the entire data set. The values for each data point are derived from fitting individual observational IDs of *RXTE* with a simple power law as explained in the text. The left panel shows the whole data set, the middle panel shows the whole data set except for the 5 flares (which are marked in Figure 1), and the right panel shows the 5 flares only. The line in each panel is a linear fit to the data, details of these fits are given in the text.

the spectral slope significantly changes within the bursts.

Using our calculated flux and spectral index data, we explore whether the orbital profiles are stable in time (in Paper I we did this for count rate only and in the wider range of 3-30 keV). To do that exploration, we divided our data into periods of 6 months each, which provided good statistics at all the phases of the orbit. The corresponding dates for each 6-month period are given in Table 1.

Figure 4 shows the evolution of the fitted flux (left panel) and the spectral index (middle panel) during these periods from top to bottom, together with the evolution of the relation between flux and spectral index (right panel), for the whole data set excluding the flares. We have reconfirmed the significant variability in the orbital profiles that was discussed in Paper I (which used only count rates). Here we also see that there is some variability in the orbital properties of the spectral index, although the significance of this variability is less dramatic, in part hampered by the large error bars. As in Figure 1, the fits in the right panel explore the possible anti-correlation between flux and spectral index, which is again better found when the data without the flares is taken into consideration.

In order to determine if this flux/spectral index anti-correlation is maintained on all timescales, we also carried out an orbit-by-orbit analysis for each of the 35 orbits covered by this data set. We found that with the available data quality, the slope of the fit to the phase resolved flux vs. the spectral index that is seen in Figure 3 is essentially maintained. The average slope obtained for this orbit-by-orbit analysis is -0.28 ± 0.04 . Thus we find that at all timescales, from observation ID, to orbital, to months, and up to years, that as flux goes up the spectral index goes down (i.e., it gets harder) and at a specific slope.

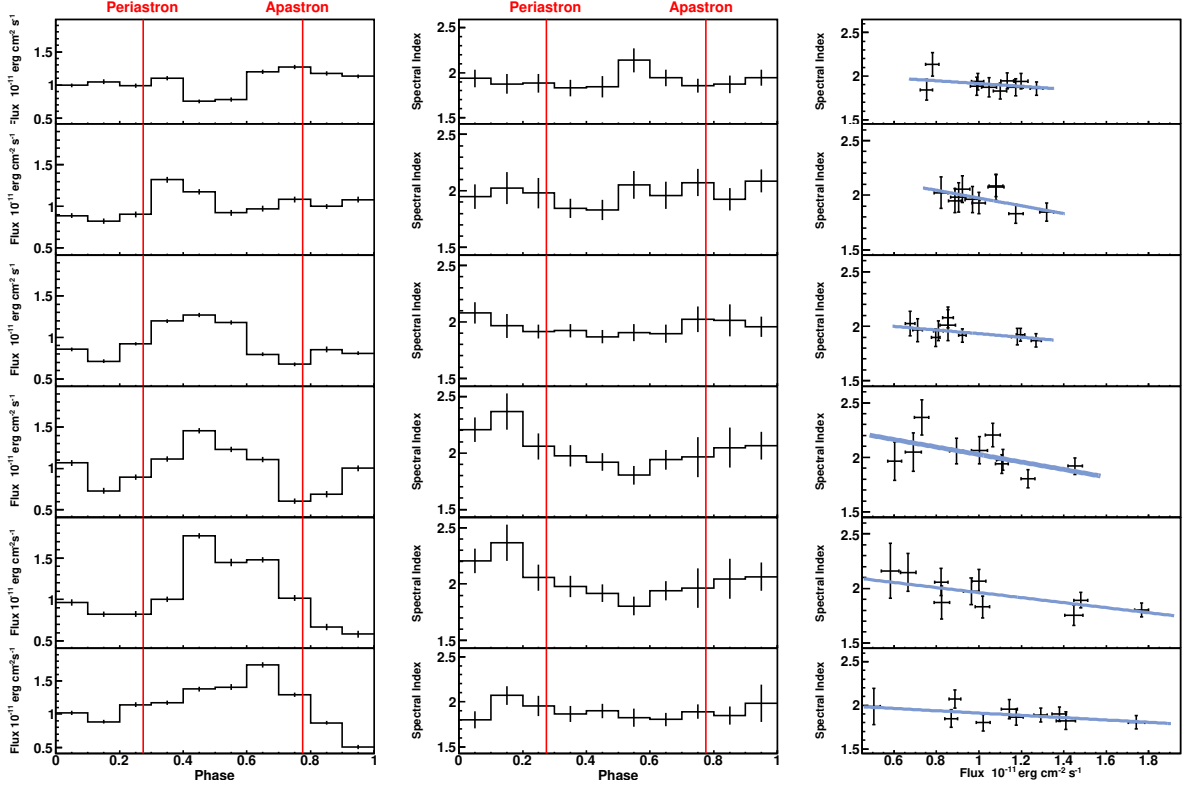


Fig. 4.— For each of the 5 separate 6-month periods considered, we show the 3-10 keV lightcurves (left) and spectral indices (middle), excluding the flares and folding at the orbital period. The right panel shows the spectral index versus flux relationship.

3.2. Flare Analysis

Besides the three flares reported by Smith et al. (2009), we here report on the two additional ones located at MJD 54670.844444 (observation ID 93102-01-25-01) and MJD 54699.653333 (observation ID 93102-01-29-01) that we have found in our data. Following the numbering of Figure 1, flares 1 through 5 happen at the LS I +61°303 phase 0.787, 0.861, 0.379, 0.651, and 0.739, respectively. While the statistics is not large, it is interesting to note that 4 out of the 5 flares are grouped in the 0.6–0.9 orbital phase bin of LS I +61°303. In total over the whole data set, there are 316 observations, and their distribution into the 10 phase bins is as follows: we have 30, 31, 36, 37, 33, 26, 33, 33, 27 and 30 observations in each of the bins (from 0–0.1, 0.1–0.2, etc.). Using this distribution, we can derive the probability of the observed configuration through the Binomial distribution. If the flares do not correlate with the orbital phase, the probability of the observed configuration is only 2.76×10^{-3} . The flare distribution in LS I +61°303 orbital phase bins might then point to

Table 1: For each 6-months time period, as described in the text and shown in Figure 4, we list the range of dates included, their corresponding MJDs, the slope of the linear fit to the data (shown in Figure 4, right panels), and the reduced χ^2 of the linear fit.

Time	Dates included	MJD	slope	reduced χ^2
1st 6-months	28/8/2007 — 28/2/2008	54340-54524	-0.21 \pm 0.21	3.7/8
2nd 6-months	29/2/2008 — 29/8/2008	54525-54707	-0.35 \pm 0.22	4.8/8
3rd 6-months	30/8/2008 — 01/3/2009	54708-54891	-0.17 \pm 0.12	3.2/8
4th 6-months	02/3/2009 — 02/9/2009	54892-55076	-0.34 \pm 0.15	11.2/8
5th 6-months	03/9/2009 — 03/3/2010	55077-55258	-0.23 \pm 0.09	5.7/8
6th 6-months	04/3/2010 — 04/9/2010	55259-55443	-0.13 \pm 0.10	4.6/8

a circumstantial evidence for an association, although statistics are still too scarce to make a definite claim.

We also looked into the spectral details of the two new flares (for the others, see Smith et al. 2009) to determine whether there is a correlation between spectral index and flux. The data on the two flares (4th & 5th) were binned based on count rate levels. The data for the 4th flare were binned into three groups with counts rates of 0–5, 5–12, and > 12 counts per second, and the flux and spectral index were derived for these groups. The data for the 5th flare were binned for count rates in the ranges 0–10, 10–18, 18–26, and > 26 counts per second. For the two flares, the spectral index versus flux relation is shown in Figure 5. Observe that the spectral index significantly varies during the flares, and that, despite the the few degrees of freedom, a linear (anti) correlation is apparent. A linear fit of 4th flare produce a slope of -0.1 ± 0.04 with a reduced χ^2 of 2.52/1, while for 5th flare produced a slope of -0.06 ± 0.01 and a reduced χ^2 of 0.46/2.

The inner structure of the flare at MJD 54670.844444 (flare 4) can be seen in Figure 7, with a time bin of 1 s. It contains several sub-flares rising and falling in the timescale of 10–20 s. The fastest flux variation lies between $t = 894$ s and 895 s where the flux increases by more than 3 times in 1 second. This does not mean that the flare itself lasts for 1 s, rather, that it contains internal variability in a few seconds timescale. The total duration of the flare is similar to those previously found by other instruments, of about 1 ks, as discussed in the introduction and below. This can be seen easily in the top panel of Figure 1, also see the zoomed view presented in Figure 6 where each point represent 64 s (top) or 16 s (bottom).

Similarly, the lightcurve of the flare at MJD 54699.653333 (flare 5), with 1 s time bins, is shown in Figure 8. Also in this case, there is internal variability in the timescales of 10–20

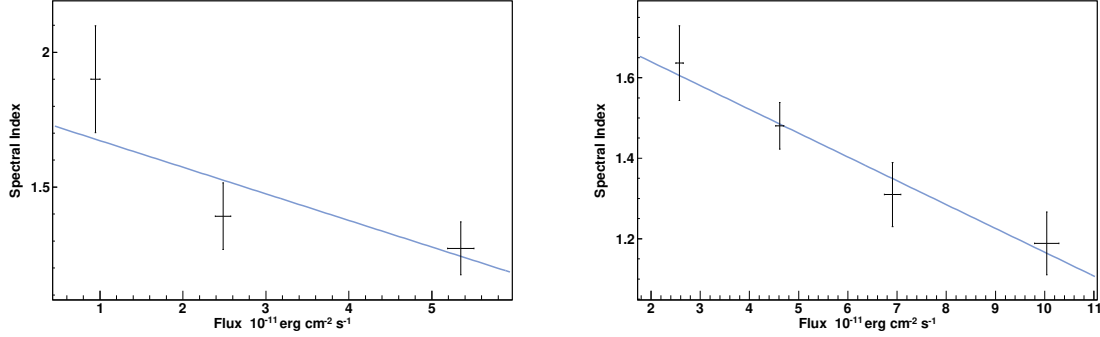


Fig. 5.— Spectral index versus flux for each of the two new flares analyzed, at MJD 54670.844444 and MJD 54699.653333, respectively. The linear fit is described in the text.

s. The peak flux of this flare is higher than that appearing at MJD 54670.844444 (flare 4). The strongest flux variation within flare 5 is situated between $t = 895$ s and 898 s, where the flux increases more than four times in these three seconds. However, note that the size of the error bars in individual data points of 1 s are large.

To study the timing properties of both flares, we derive lightcurves from Good Xenon Data with time resolution at 0.01 seconds and then obtained a power spectrum. The result of timing analysis of these flares is shown in Figure 9. The power spectrum for MJD 54670.844444 (flare 5) show no evidence for the existence of any structure in the power spectrum while the power spectrum for MJD 54699.653333 (flare 5) appears to show an QPO-like structure at around 2 Hz. In order to test the significance of this feature, we fit the power spectrum with two Lorenz profiles (one to match the low frequency rise) and a constant. The χ^2 of the fit is 177.4 under 189 degrees of freedom; with the fitting parameters for the QPO being a central frequency equal to 2.115 ± 0.015 , a width of 0.103 ± 0.259 , and a normalization of 0.698 (error cannot be well constrained). To test whether the QPO is significant we also fit the power spectrum with just one Lorenz profile (to match the low frequency rise) and a constant (i.e., removing the putative QPO), deriving a χ^2 of 185.7 with 192 dof. We carried out an F-test between the two fits.

The F-statistic value is 2.94 and the probability for rejecting the existence of the QPO is 0.034. Thus, we conclude that this seeming QPO is not significant. Besides that, we explored whether the significance increases in different energy bands. The signal seems stronger in the 1.5–20 keV band, with an F-statistic value of 6.60 and rejecting probability at 2.897×10^{-4} , implying a pre-trail significance roughly of 3.5σ . In this energy range other similar peaks do appear in the power spectrum, reducing the case for a real QPO appearing irrespective of the energy cut even further. We caution that the existence of this QPO structure is mentioned

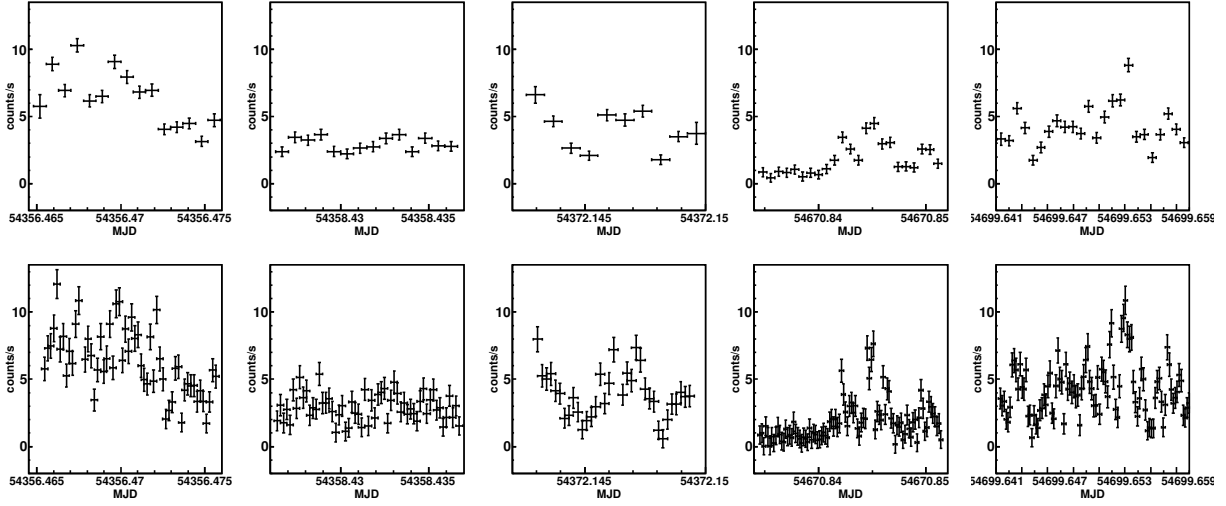


Fig. 6.— Zoom in the lightcurve presented in the top panel of Figure 1 for each of the 5 flares detected by PCA. Each point represents 64 s in the top panels and 16 s in the bottom panels.

in the ATel 1730 by Ray et al. (2008) and assumed as real in the literature already, see Massi & Zimmermann (2010). Our results discourage this assumption.

3.3. Possible super-orbital influence

The modulated flux fraction (obtained as $(c_{max} - c_{min}) / (c_{max} + c_{min})$, where c_{max} and c_{min} are the maximum and minimum counts rate in 3–30 keV in the orbital profile, after background subtraction) changes as a function of time. We here consider whether it maybe correlated with the super-orbital radio period (1667 ± 8 days, Gregory 2002). We take the reference time of the zero phase at MJD 43366.275 and the shape of the outburst peak flux modulation estimated by Gregory (2002) in radio. We fit this shape with a 1667 ± 8 period sine function (see Figure 10, left panel), finding (not unexpectedly) that it could represent the radio super-orbital evolution well.

At each of the timescales considered (4, 5, 6, 7, and 9 months) we computed the modulated flux fraction from the counts rate in 3–30 keV as described above and found that as soon as timescales are long enough compared with the orbital period, so that orbit-to-orbit variations do not play a role, there is essentially a monotonically increasing trend of the modulated fraction. This is shown in the middle panel of Figure 10.

If we fit the modulation fraction values with the sine function mentioned above, no

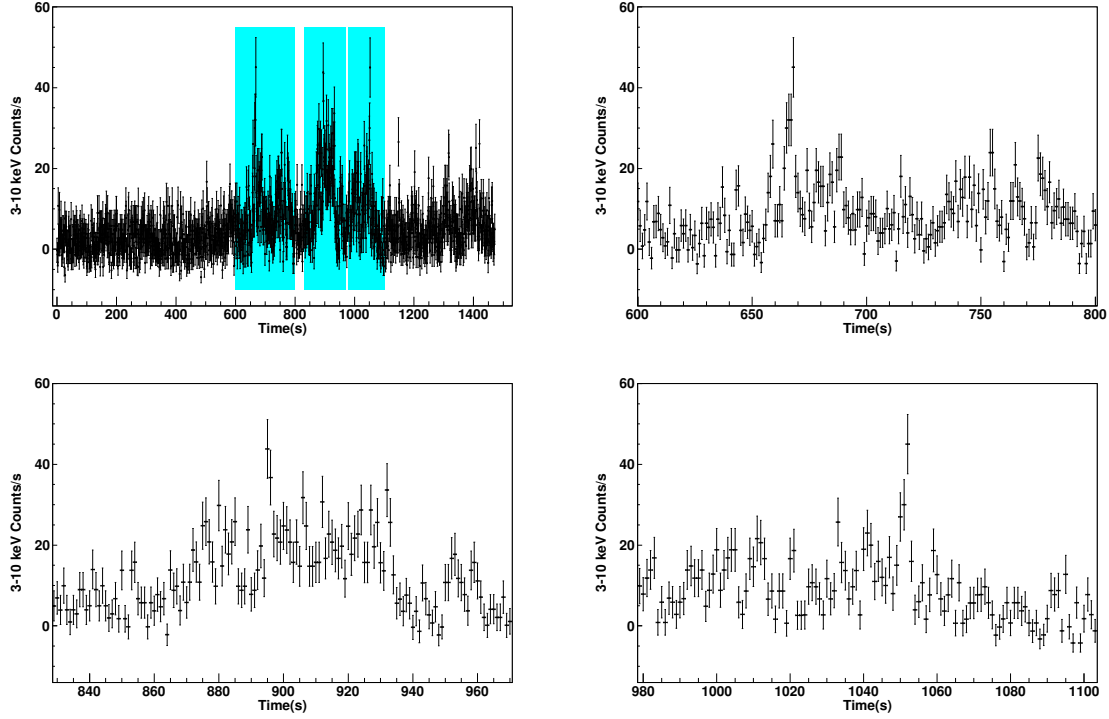


Fig. 7.— Top left panel: Lightcurve of the flare at MJD 54670.844444 (flare 4) binned in 1 s intervals with $t = 0$ at the beginning of the time period; count rates are obtained from the top layer of PCU 2, 3 and 4 in the 3–10 keV. The top right panel shows a zoom from $t = 600$ s to 800 s. The bottom panels show zooms from 829 s to 970 s and 979 s to 1102 s, respectively. The color shadow in the top left shows the zoomed time spans. Note that the mean value of the flux more than triples in 1 second from $t = 894$ s to 895 s showing internal variability.

apparent correlation with the super-orbital radio period is found, at least with the data at hand (covering already > 0.5 of the super-orbital period). For instance, the modulation fraction of each of the periods of 6-months were fitted with the above-mentioned sine function (results can be seen in Figure 10, right panel, black line) and we derived a reduced χ^2 of 14.04/4, much worse than reduced χ^2 of just a straight line fit, 2.19/4.

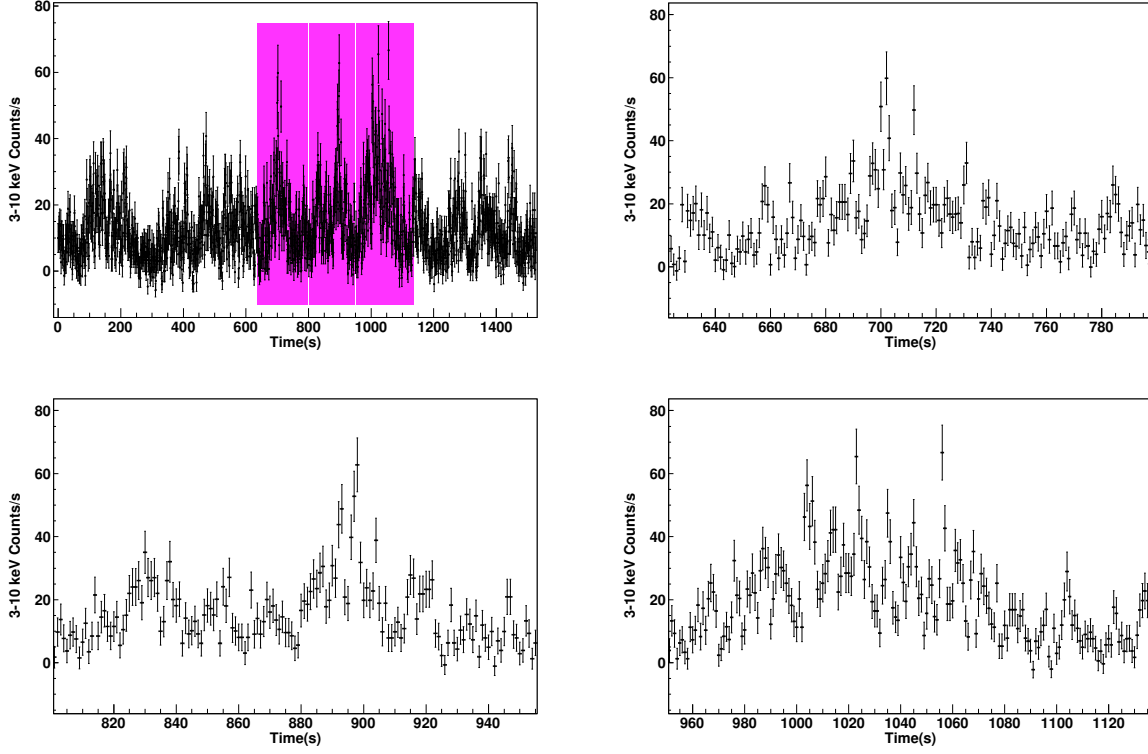


Fig. 8.— Top left panel: Lightcurve of the flare at MJD 54699.653333 (flare 5) binned in 1 s intervals with $t = 0$ at the beginning of the time period; count rates are obtained from the top layer of PCU 2, 3 and 4 in the 3–10 keV. The top right panel shows a zoom from $t = 600$ s to 800 s. The bottom panels show zooms from 800 s to 960 s and 960 s to 1120 s, respectively. The color shadow in the top left shows the zoomed time spans, as in Figure 7. Note that the flux more than triples in 1 second from $t = 895$ s to 898 s showing internal variability.

4. Discussion

4.1. On the spectral index versus flux

The data collected with the PCA detector can be described (at all scales) by a featureless power-law spectrum with photon indices varying along the orbit, depending on the flux state. Contrary to the typical low-hard and high-soft states of XRBs, both hosting a neutron star or a black hole, we confirm here earlier hints that there is a strong correlation between spectral index and flux presenting itself in the opposite direction. For LS I +61°303, the spectral index value is anti-correlated with the flux level (otherwise stated, the spectral hardness is directly correlated with the flux level). The correlation seems linear, under scrutiny of

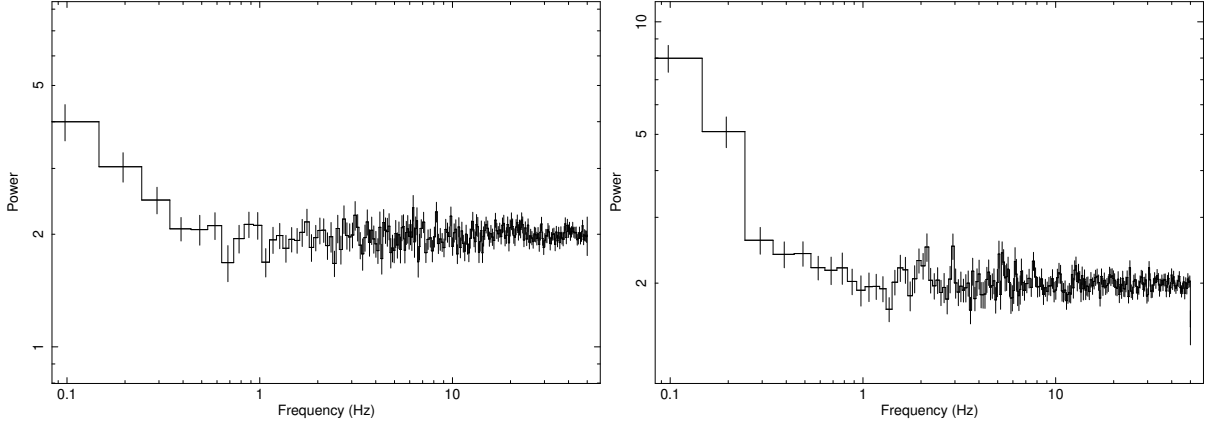


Fig. 9.— Left: Power spectrum of the flare found at MJD 54670.844444 (flare 4) as described in the text. Right: Power spectrum of the flare at MJD 54699.653333 (flare 5). No statistically significant structures are found. See the discussion in the text.

current statistics, and present across all flux states of the source and all phenomenological timescales found. This anti-correlation was hinted at in *XMM* observations (48.7 ks, around orbital phase 0.6, Sidoli et al. 2006), and in *Chandra* (50 ks observations near orbital phase 0.04, Paredes et al. 2007, 95 ks observations from orbital phase 0.94 to 0.98); in addition of the already commented work by Smith et al. (2009) using PCA data (a sub-set of the study presented here). Earlier data is consistent with this now-proven trend; see, for example, the hardness ratio values plotted as figure 3 in the work of Taylor et al. (1996).

The spectral index - flux trend has also been found for another source, LS 5039, whose overall features across the electromagnetic spectrum make it very similar to LS I +61°303. Bosch-Ramon et al. (2005) found a similar tendency in fluxes and photon indices, although the data were background contaminated by diffuse X-ray emission from the Galactic Ridge (Valinia et al. 1998), likely preventing a proper photon index determination. Nonetheless, Takahashi et al. (2009) confirmed the trend, and showed a harder-when-brighter behavior of LS 5039 using Suzaku observations along its orbit. However, despite this similarity between LS I +61°303 and LS 5039, Kishishita et al. (2009) reported that the latter source has a X-ray lightcurve presenting long-term stability using multi-satellite observations between 1999 and 2007. For LS 5039, even fine structures in the lightcurves such as spikes and dips are found to be quite similar from one orbit to another, which is quite different from the LS I +61°303 behavior we find. The most appealing explanation for such a distinction is that the different behavior of the lightcurves arises from the stellar object, especially given the lack of knowledge about the nature of the compact object in both systems. While LS 5039 hosts an O star, LS I +61°303 has a Be star primary, which is characterized with a dense equatorial disk. If, for instance, there are disc structure changes in time, the latter may

induce variability in X-ray modulation. Admittedly, it could also be that the compact objects are different. Pulsar composed systems could provide feasible scenarios for a clocklike X-ray emission (e.g., see Dubus 2006; Sierpowska-Bartosik & Torres 2008), devoid of possible variability found in the low-hard state of black-hole composed systems where the jet is thought to be connected to disc accretion, instabilities of which would lead to X-ray changes.

To address the issue of the origin of the X-ray emission, the fact that there is no accretion disc signature in our data, nor it is apparent in any other dataset of LS I +61°303 (see, for instance, Rea et al. 2010), as well as the lack of a cutoff in the X-ray spectra up to 30 keV as we find here, or in the *INTEGRAL* range (see Zhang et al. 2010), may not favour the X-ray radiation origin as thermal Comptonization of a corona. Therefore, our observations emphasize that the origin of the X-ray emission may be due to inverse Compton (IC) and/or synchrotron processes. The hardness increase with flux level may be explained differently depending on the underlying model for the system, but in principle both can accommodate it. In jet models like the one posed by Bosch-Ramon et al. (2006), an increase in accretion rate would imply a higher electron acceleration efficiency in the jets. There would be more particles at the higher-energy range of the electron energy distribution, and this would lead to a hardening of the X-ray spectrum. The fact that the maximum of the flux (the hardest spectrum) does not occur at periastron makes this interpretation more complex but still possible. On the other hand, in models where the X-ray emission arises as a result of IC scattering of ultrarelativistic electrons accelerated at the pulsar wind termination shock (for which losses scale with the distance to the massive star), it is the complex interplay of the different losses at hand with the acceleration efficiency that makes the maximal energy of electrons to vary along the orbit. Investigating the conditions for the particle propagation in the shock region requires setting the parameters defining the local magnetic field and the thermal field densities. The former scales with the distance from the pulsar site, whereas the latter scales with the distance from the massive star. Assuming LS I +61°303 parameters (even within the influence of their uncertainties, see, e.g., Sierpowska-Bartosik & Torres 2009), and reasonable assumptions for the decay of the pulsar magnetic field out of the magnetosphere, one can compute all timescales for the losses involved (see e.g., Khangulyan et al. 2007 for a similar case in the system PSR B 1259-63); and use them to analyze the maximal energies of shock-accelerated electrons, finding that these are the highest for phases around apastron of LS I +61°303. The extension of the electron spectra to higher energies may thus reflect on a harder, more luminous X-ray flux. In addition, if the pulsar wind moves through the region of varying density of the equatorial wind of the Be star, during its passage through the densest parts of the disk, X-ray emission may also be affected by Coulomb losses and adiabatic cooling of the accelerated particles, helping in the orbital modulation of the X-ray flux.

4.2. On the flares

Flares from LS I +61°303 at timescales of hours are known since long. For instance, Harrison et al. (2000) detected source variations of about 50% on timescales of half an hour. Sidoli et al. (2006) also found evidence for a rapid (again, on timescales of few hours) change in flux and hardness ratio: the source flux changed by a factor of 3 within 1 ks in their *XMM*-Newton observations, and by a factor of ~ 4 within 1.5 ks in their Beppo-SAX observations. Esposito et al. (2007) found a similar behavior in Swift/XRT data, and Paredes et al. (2007) found another miniflare over a timescale of 1 ks (with a total duration of 3 ks), with the count rate increasing by a factor of 2. Rea et al. (2010) found, in *Chandra* data, two flares lasting 3 and 1.5 ks with a rise-time of approximately 100 s. Due to their high angular resolution, *Chandra* and *XMM* observations provide certainty that the origin of this variability is LS I +61°303.

We also observed significant flux fluctuations in our PCA data. In total, 5 flares were detected by PCA and are shown in Figure 1 both in count rate and in fitted flux. Smith et al. (2009) independently reported on some of them, the earliest, while analyzing the initial part of this dataset. The overall features of all PCA flares are very similar one to another: in 1 s-binned lightcurves there is significant structure, we can see the flux rising up to 3 times in a single or a few bins (albeit each point has large error bars); with the whole flare lasting up to the order of ks. Yet, the shortest of the bursts detected on LS I +61°303 observations has been made with Swift-BAT, which reported the detection of a short (0.23 s), 10^{37} erg (if at the distance of LS I +61°303) in the 15–150 keV energy range (Barthelmy et al. 2008). Swift-XRT showed no increased flux from the direction of LS I +61°303, just 921 s later. Was this an unlucky coincidence of a short unrelated GRB seen through the galaxy? Or was this emission also coming from LS I +61°303? Was this magnetar activity (see Dubus & Giebels 2008)? And in the latter case, how is the wind needed in all currently known pulsar models generating TeV emission maintained? Why is there radio emission from LS I +61°303, unlike all known magnetars? Where is the region of generation of accelerated particles? Maintaining that LS I +61°303 is the first magnetar in a binary might necessarily lead to a complete reworking of the basic ideas for high-energy emission generation, since the pulsar wind zone or the pulsar wind – stellar wind shock-induced particle acceleration cannot stand vis-a-vis.

Magnetars do show X-ray flaring activity on several time-scales, but they are not rotational-powered; their emission (flaring and persistent) is due to the presence and instability of their ultrastrong magnetic fields (see Mereghetti 2008 for a recent review).³ No

³It is interesting to note in passing that a similar ~ 1 ks timescale variability has been found –also using

magnetar has been found in GeV gamma-rays (Abdo et al. 2010); less in TeV. However, the models of (accreting) magnetars in binaries have been presented by Bozzo et al. (2008) and Bednarek (2009). In Bednarek (2009) models, the matter from the stellar wind penetrates the inner magnetosphere of the magnetar up to the point in which the magnetic pressure balance the gravitational pressure of the accreting matter creating a turbulent region, suggested to be prone to the acceleration of electrons to relativistic energies (the propeller phase). General features of the model seem in accord with the overall phenomenology, albeit the X-ray and the GeV emission are overpredicted in comparison with Fermi and our *RXTE* data.

In the accretion scenario flares are easily explainable as changes in the accretion rate from the companion star or the accretion disc about the compact object. Flares of such different timescales are not uncommon in accretion-based systems such as microquasars. In the rotational-powered pulsar scenario, the variability we observe would require clumpiness of the Be stellar wind, where the size, mass, and number density of the clumps imprint their signal on the X-ray emission (see Zdziarski, Neronov & Chernyakova 2008, Rea et al. 2010). It does not appear contrived that clumps of the order of 10^{11} cm or smaller could be related with the variability found in PCA data, and similarly, with 1-ks timescales. For smaller timescales, other processes –likely depending on the nature of the companion– probably have to be invoked. We note that X-ray observations of LS 5039 (e.g., Bosch-Ramon et al. 2005) hourly timescale flux variations are similar to what we find for LS I +61°303, but not faster variability.

4.3. On the variability of orbital profiles

As it shown here and in Paper I, orbital profile variability is seen from orbit-to-orbit all the way up to multi-year timescales. The phase of the profile maximum also changes. The study of short-term, simultaneous multifrequency observations such as the one made by the MAGIC Collaboration (Anderhub et al. 2009) showed an X-ray – TeV correlation. Is it sustained in time? In Paper I we have already noted that given the variability found in X-rays, the correlation shown by Anderhub et al. (2009) in about half an orbit produces local-in-time information useful for determining the process or the primaries responsible for the radiation detected, but probably it is not enough to establish an overall behavior. In fact, given the variable nature of the X-ray emission, a correlation found in a short observation

PCA– in the high mass X-ray binary 2S 0114+650 and it was also ascribed to a clumping wind (Farrel et al. 2008). 2S 0114+650 contains a super-slow rotator, one of the slowest spinning X-ray pulsars yet discovered (2.7 hours), which have also been assessed as a possible magnetar (Li & van den Heuvel 1999).

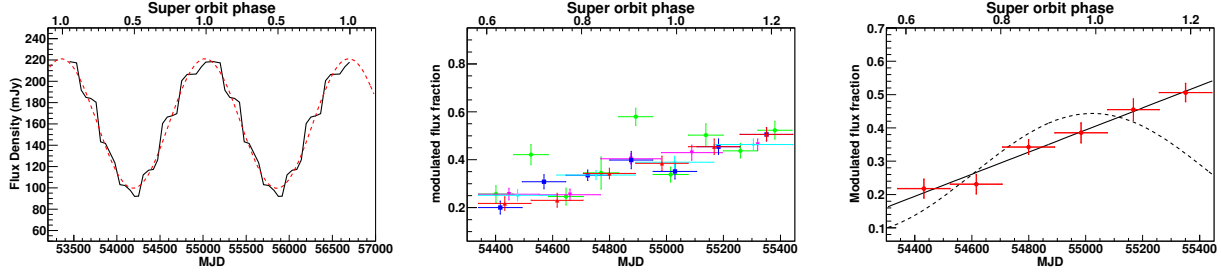


Fig. 10.— The left panel shows the shape of the peak flux modulation in radio (black line) and the fitting with a sine function (dotted red line). The middle panel shows the evolution of the modulated fraction at different timescales (4, 5, 6, 7, and 9 months). The size of the error along the x-axis of each of the data points gives account of the timescales considered. The black line in right panel shows the linear fitting to the 6-months modulated flux fraction data. The dotted line in right panel shows the fitting with the sine function in left panel.

might not be a sufficient proof that this correlation maintains with time. However, if the TeV and X-ray emission are indeed always correlated, the TeV maximum should also vary in phase, affected by the different level of absorption at which the maximal photon production happens. TeV and X-ray correlations could be explained, for instance, assuming dominant adiabatic losses (see, e.g., Zabalza et al. 2010). However, if such is the case, it would be highly unlikely to have whole orbits with only upper limits in the TeV range, while maintaining the X-ray emission level. This is apparently the case, as recent observations of VERITAS and MAGIC has shown that the source can turn off at TeV energies (Aliu et al. 2011, Jogler 2010). In fact, no TeV emission has been reported since summer 2008, when the source re-appeared at periastron, emphasizing the variability of the TeV maximum phase-position (Ong et al. 2010). The adiabatic-losses one-zone model has in addition the caveat of severely overproducing (unless a low-energy cutoff of the electron distribution is introduced ad-hoc) the GeV fluxes measured by Fermi (by 2-3 orders of magnitude). However, the 1–10 GeV data points by Fermi are at a much lower level than predicted by models, in general.

5. Summary

We reported here on the full analysis of a Rossi X-ray Timing Explorer (*RXTE*) Proportional Counting Array (PCA) monitoring of the γ -ray binary system LS I +61°303. The data set covers 42 contiguous cycles of its orbital motion. A detailed discussion on the count rate variability across different timescales can be found in Paper I; although we have extended further this analysis with additional orbits in order to consider the possible appearance of the super-orbital modulation. In here, we focused on the spectral properties and the analysis

of two new flares appearing in these data set. The following is a summary of our findings.

- The soft X-ray emission from LS I +61°303 presents a periodic behavior at the orbital period, whose shape varies at all timescales explored. Profile variability is seen from orbit-to-orbit all the way up to multi-year timescales. The phase of the profile maximum also changes (see Paper I for an initial analysis in this sense). The study of simultaneous (part of one orbit) multifrequency observation showed a X-ray – TeV correlation, but no evidence that it remains valid in time (Anderhub et al. 2009). TeV and X-ray correlations could be explained, for instance, assuming dominant adiabatic losses (see, e.g., Zabalza et al. 2010). However, if such is the case, it would be unlikely to have whole orbits with only upper limits in the TeV range, while simultaneously maintaining the X-ray emission level – as found here to be the case along several years.
- There were a total of 5 flares found on top of the typical behavior of LS I +61°303. These flares, due to the large PCA field of view, may or may not be associated with LS I +61°303, but given earlier *XMM* and *Chandra* observations finding similar ks phenomenology, it is likely they are. 4 out of the 5 flares are grouped in the 0.6–0.9 orbital phase bin of LS I +61°303. If the flares do not correlate with the orbital phase, the possibility of the resulting configuration is 2.76×10^{-3} . This may be indicative of an association, but certainly not a compelling proof. The inner structure of the flares present significant variability in shorter-than-1 ks timescales. Timing analysis of the flares does not show any structure in the power spectrum. The previously claimed QPO in the 5th flare is not statistically significant. Flares can be generated by changes in the mass loss rate of the star or clumpiness of the Be stellar wind.
- There is moderate variability of the spectral index across the 3 year observation period. We significantly confirmed the hints for an anti-correlation (now at $\sim 10.2\sigma$) between spectral index and flux, detecting a harder-when-brighter behavior of the source. This could be explained differently by jet models and pulsar wind models. Our observation emphasizes that the X-ray emission may be due to inverse Compton and/or synchrotron processes, rather than thermal Comptonization of a corona.
- We explored the possible appearance of the super-orbital influence on the modulated fraction of the X-ray emission, with no clear detection of such a modulation in the X-ray band. Future data may perhaps clarify on this issue.

This work was subsidized by the National Natural Science Foundation of China, the CAS key Project KJCX2-YW-T03, and 973 program 2009CB824800. Jianmin Wang and

Shu Zhang thank the Natural Science Foundation of China for support via NSFC-10325313, 10521001, 10733010, 11073021 and 10821061. We acknowledge support from the grants AYA2009-07391 and SGR2009-811, as well as the Formosa Program TW2010005. This work was also partially supported by NASA DPR No. NNG08E1671. Nanda Rea is supported by a Ramony Cajal Fellowship. We thank the referee for a careful reading of the manuscript.

REFERENCES

- Abdo A. et al. 2009, ApJ 701, L123
- Abdo A. et al. 2010, ApJ 725, L73
- Acciari, V. et al. 2008, ApJ 679, 1427
- Acciari, V. A. et al. 2009, ApJ 700, 1034
- Aharonian, F. et al. 2005a, Science 309, 746
- Aharonian, F. et al. 2005b, A&A 442, 1
- Aharonian, F. et al. 2006, A&A 460, 743
- Albert, J. et al. 2006, Science 312, 1771
- Albert, J. et al. 2007, ApJ 665, L51
- Albert, J. et al. 2007b, ApJ 663, 125
- Albert, J. et al. 2008, ApJ, 684, 1351
- Aliu, et al. 2011 in Proceedings of the 1st Session of the Sant Cugat Forum of Astrophysics: ICREA International Workshop on the High-Energy Emission from Pulsars and their Systems, Nanda Rea & Diego F. Torres (Editors), Springer, ISSN: 1570-6591, in press.
- Anderhub, H. et al. 2009, ApJ 706, L27
- Aragona, C., McSwain, M. V., Grundstrom, E. D., Marsh, A. N., Roettenbacher, R. M., Hessler, K. M., Boyajian, T. S., & Ray, P. S. 2009, ApJ 698, 514
- Valinia, A. & Marshall, Francis E. 1998, ApJ 505, 134
- Barthelmy, S. et al. 2008, GCN, 8215
- Bednarek, W. 2009 MNRAS 397, 1420

- Bosch-Ramon, V., Paredes, J. M., Riból, M., Miller, J. M., Reig, P., & Martí, J. 2005, *ApJ* 628, 388
- Bosch-Ramon, V., Paredes, J. M., Romero, G. E., & Riból, M. 2006, *A&A* 459, 25
- Bozzo, E., Falanga, M., & Stella, L. 2008, *ApJ* 683 1031
- Casares, J., Ribas, I., Paredes, J. M., Martí, J., & Allende Prieto, C. 2005, *MNRAS* 360, 1105
- Chernyakova, M., Neronov, A., & Walter, R. 2006, *MNRAS* 372, 1585
- Dhawan, V., Mioduszewski, A., & Rupen, M. 2006, *Proceedings of the VI Microquasar Workshop: Microquasars and Beyond*. September 18-22, 2006, Como, Italy., p.52.1
- Dubus, G. 2006, *A&A*, 456, 801
- Dubus, G., & Giebels, B. 2008, *Astron. Tel.*, 1715
- Esposito, P., Caraveo, P. A., Pellizzoni, A., de Luca, A., Gehrels, N., & Marelli, M. A. 2007, *A&A* 474, 575
- Farrell, S. A., Sood, R. K., O’Neill, P. M., & Dieters, S. 2008, *MNRAS* 389, 608
- Filippova, E. V., Tsygankov, S. S., Lutovinov, A. A., & Sunyaev, R. A., 2005, *Astron. Lett.*, 31, 729
- Gregory, P. C. 2002, *ApJ* 575, 427
- Grundstrom, E. D. et al. 2007, *ApJ* 656, 437
- Jogler, T., talk presented at the ”Galactic Variable Source Workshop” Heidelberg November 30 – December 3, 2010
- Harrison, F. A. 2000, *ApJ* 528, 454
- Hutchings, J. B., & Crampton, D. 1981, *PASP* 93, 486
- Kalberla, P. M. W., Burton, W. B., Hartmann, D., Arnal, E. M., Bajaja, E., Morras, R., & Pöppel, W. G. L. 2005, *A&A* 440, 775
- Khangulyan, D., Hnatic, S., Aharonian, F., & Bogovalov, S. 2007, *MNRAS* 380, 320
- Kishishita, T., Tanaka, T., Uchiyama, Y., & Takahashi, T. 2009, *ApJ* 697, L1

- Li, X-D., & van den Heuvel, P. J. 1999, *ApJ Letters* 513, L45
- McClintock, J. E., & Remillard, R. A. 2003, in Lewin W. H. G., van der Klis M., eds, *Compact Stellar X-ray Sources*. Cambridge Univ. Press, Cambridge
- Maraschi, L., & Treves, A. 1981, *MNRAS* 194, 1
- Massi, M., Ribó, M., Paredes, J. M., Garrington, S. T., Peracaula, M., & Martí, J. 2004, *A&A* 414, L1
- Massi, M., & Zimmermann, L. 2010, *A&A* 515, 82
- Mendelson, H., & Mazeh, T. 1989, *MNRAS* 239, 733
- Mereghetti, S. 2008, *A&AR*, 15, 225
- Ong, R. A. et al. 2010, *Astron. Tel.*, 2948
- Paredes, J. M. et al. 1994, *A&A* 288, 519
- Paredes, J. M., Marti, J., Peracaula, M., & Ribo, M. 1997, *A&A* 320, L25
- Paredes J. M., Ribo, M., Bosch-Ramon, V., West, J. R., & Butt, Y. M. 2007, *ApJ* 664, L39
- Rea, N., Torres, D. F., van der Klis, M., Jonker, P. G., Méndez, M., & Sierpowska-Bartosik, A. 2010, *MNRAS* 405, 2206
- Rea, N., & Torres, D. F. 2008, *Astron. Tel.*, 1731
- Sidoli, L., Pellizzoni, A., Vercellone, S., Moroni, M., Mereghetti, S., & Tavani, M. 2006, *A&A* 459, 901
- Smith, A., Kaaret, P., Holder, J., Falcone, A., Maier, G., Pandel, D., & Strohm, M. 2009, *ApJ* 693, 1621
- Takahashi, T. et al. 2009, *ApJ* 697, 592
- Tavani, M. et al. 1996, *A&AS* 120, 243
- Taylor, A. R., & Gregory P. C. 1984, *ApJ* 283, 273
- Taylor, A. R., Young, G., Peracaula, M., Kenny, H. T., & Gregory, P. C. 1996, *A&A* 305, 817
- Torres, D. F. et al. 2010, *ApJ* 719, L104 (paper I)

- Sierpowska-Bartosik, A., & Torres, D. F. 2008, *Astropart. Phys.*, 30, 239
- van Dijk, R. et al. 1996, *A&A* 315, 485
- Zamanov, R. K., Martí, J., & Paredes, J. M. et al. 1999, *A&A* 351, 543
- Zhang, S., Torres, D. F., Li, J., Chen, Y. P., Rea, N., & Wang, J. M. 2010, *MNRAS* 408, 642
- Zdziarski, A. A., Neronov, A., & Chernyakova, M. 2008, *arXiv:0802.1174*
- Zabalza, V., Paredes, J. M., & Bosch-Ramon, V. 2010, *arXiv 1011.4489*